Structural Variations and Bonding in Gold Halides: A Quantum Chemical Study of Monomeric and Dimeric Gold Monohalide and Gold Trihalide Molecules, AuX, Au_2X_2, AuX_3, and Au_2X_6 (X = F, Cl, Br, I)

Axel Schulz*[b] and Magdolna Hargittai*[a]

Abstract: The molecular structures of all gold mono- and trihalides and of their dimers have been calculated at the B3LYP, MP2, and CCSD(T) levels of theory by using relativistic pseudopotentials for all atoms except fluorine. Our computations support the experimental observation that the relative stability of the monohalides increases from the fluoride toward the iodide, while the stability trend of the trihalides is the opposite. The potential energy surface (PES) of all gold trihalides has been investigated. These molecules are typical Jahn–Teller systems; the trigonal planar D_{3h}-symmetry geometry does not correspond to the minimum energy structure for any of them. At the same time, the amount and character of their Jahn–Teller distortion changes gradually from AuF_3 to AuI_3. The minimum energy geometry is a T-shaped structure for AuF_3 and $AuCl_3$, with a Y-shaped transition-state structure. For AuI_3, the Y-shaped structure lies lower than the T-shaped structure on the PES. For $AuBr_3$ and AuI_3, neither of them is the global minimum but instead an L-shaped structure, which lies outside the Jahn–Teller PES. This structure can be considered to be a donor–acceptor system, or a closed-shell interaction, with I_2 acting as donor and AuI as acceptor. The dimers of gold monohalides have very short gold–gold distances and demonstrate the aurophilic interaction. The dimers of the trihalides are planar molecules with two bridging halogen atoms.

Keywords: gold · halogens · hypervalent compounds · Jahn–Teller distortion · metal–metal interactions

Introduction

Gold halides are interesting and challenging examples to study structural and bonding peculiarities. However, they are difficult objects for both experimental and computational studies, even with today's sophisticated techniques. Gold monohalides are probably the ultimate examples of relativistic effects on structural parameters, as the relativistic contraction reaches a maximum with the filled 5d shell of gold.[1] Their dimers, with their extremely short Au···Au distances, are the best examples of the metallophilic interaction[2] between metals with d^{10} electronic configuration, having earned their own name "aurophilic interaction".[3] These attractive interactions are just one of the many unexpected closed-shell interactions in inorganic chemistry.[4]

The gold trihalides are subject to the Jahn–Teller effect,[5] which is one of the intriguing phenomena in chemistry. It tells us that nonlinear systems in degenerate electronic states will be unstable and, therefore, spontaneously distort to a lower symmetry configuration, thereby removing the electronic degeneracy. Owing to the very nature of the effect, which involves the coupling of the electronic and vibrational motions of the molecule, a Jahn–Teller molecule is a basically dynamic system. This is one of the reasons why it has been mostly observed in crystals in which the so-called Jahn–Teller cooperativity[6] enhances it into a static effect and makes it experimentally observable. Their detection in the gas phase is more difficult.

It is generally supposed that even if there is a Jahn–Teller distortion in a molecule, the symmetry of the ground state will still be the same as that of the undistorted initial degenerate state, that is, higher than the symmetry of the structure to which the molecule distorts.[7, 8] This is due to the highly dynamic nature of these systems and to tunneling effects. The relative magnitude of the timescale of the vibronic interac-

[a] Prof. Dr. M. Hargittai
Structural Chemistry Research Group
Hungarian Academy of Sciences
Eötvös University, Pf. 32, 1518 Budapest (Hungary)
Fax: (+36) 1-372-2731
E-mail: hargittaim@ludens.elte.hu

[b] Dr. A. Schulz
Department of Chemistry, LMU, University of Munich
Butenandtstrasse 5–13 (Haus D), 81377 Munich (Germany)
E-mail: lex@cup.uni-muenchen.de

Supporting information for this article is available on the WWW under http://wiley-vch.de/home/chemistry/or from the author. The Supporting Information includes the absolute energies and frequencies of all species, activation energies and geometries of the transition states, the HOMO/LUMO energies of AuX and X_2, and the orbital energies and gaps.

  0947-6539/01/0717-3657 $ 17.50+.50/0

tions and the timescale of the measurement by a particular experimental technique is of importance here. In this respect, we have to distinguish between the so-called static and dynamic Jahn–Teller distortions. In the most frequent dynamic cases, the molecule distorts from the high-symmetry configuration to a lower symmetry one along the vibrational coordinate for which the vibrational degrees of freedom are nonzero at the symmetric configuration. This distortion lifts the degeneracy and the potential energy surface (PES) for such a system is of the "Mexican hat" type, with the high-symmetry configuration at the center (maximum) and the distorted one around the brim of the hat (minimum). If there is only linear vibronic coupling (that is, without higher order coupling), the PES will be the same around the brim of the hat, so the molecule can freely move around this minimum. In such a dynamic Jahn–Teller case the molecule is not localized at a particular point on the PES, and the higher symmetry of the undistorted degenerate structure can be considered the symmetry of the ground electronic state.

There are cases, however, when in addition to the linear vibronic coupling, quadratic coupling becomes large enough to cause the appearance of local saddle points along the brim of the hat in between the minimum positions (for a trigonal $E \times e$ case, three of them). If the energy difference between these local minima and the saddle points is large enough, the molecule may be locked into the minimum positions, and the ground-state symmetry of the molecule will be nondegenerate. Recent theoretical calculations for $E \times e$,[9] $T \times t_2$,[10] and also for $H \times h$[11] systems showed that with large enough quadratic coupling the ground state becomes nondegenerate. These are cases of the static Jahn–Teller distortion, and for such molecules even a gas-phase experiment may measure the distorted nongenerate ground-state geometries; an example of this is the electron diffraction study of MnF_3.[12]

Gold trihalides exhibit a strong Jahn–Teller effect, as was shown earlier for AuF_3 by electron diffraction experiments[13] and for both AuF_3 and $AuCl_3$ by computations.[13–15] The electron diffraction study of AuF_3, as in case of MnF_3, proved beyond doubt that the distortion of the molecule is static in nature; even at the high experimental temperature, over 1000 K, the F···F peak of the radial distribution splits, which indicates a lower than trigonal symmetry for the average structure of the molecule.

The description of Jahn–Teller systems by computation is rather involved. The Jahn–Teller PES presents a conical intersection between two electronic states, and the description of the high-symmetry degenerate structure is not without difficulties.[16, 17] The best way to calculate this point is by multiconfigurational methods, such as the complete-active-space self-consistent-field (CASSCF) method. Only recently have methods been suggested to calculate spectroscopic Jahn–Teller parameters by ab initio methods for dynamic Jahn–Teller cases.[18] For a comprehensive discussion of vibronic-coupling theory we refer to the monograph by Bersuker and Polinger.[6]

Gold iodides have received considerable interest recently. It has been shown that gold iodides with excess iodine can be used as substitutes in polyiodide networks, and this may open up a new area of host–guest chemistry.[19] This brings up the possible similarity of their bonding. I_3 and its ions were studied recently by Hoffmann et al.,[20] who showed that the bonding in these systems can be equally well described by donor–acceptor bonding and by hypervalent, electron-rich, three-center bonding.

Abstract in Hungarian: *Arany-mono- és trihalogenidek monomerjeinek és dimerjeinek a molekulaszerkezetét számítottuk ki B3LYP, MP2 és CCSD(T) szinten, pszeudopotenciálok alkalmazásával mindegyik atomon, kivéve a fluort. Számításaink alátámasztják azt a kísérleti megfigyelést, hogy az arany-monohalogenidek stabilitása a fluoridtól a jodid felé nő, míg a trihalogenideké ebben az irányban csökken. Az összes arany-trihalogenid potentiális-energia felületét megvizsgáltuk. Ezek a molekulák tipikus Jahn–Teller torzult rendszerek; a D_{3h} szimmetriájú szerkezet egyikük esetében sem minimum. A Jahn–Teller torzulás mértéke fokozatosan csökken a fluoridtól a jodid felé haladva. Az AuF_3 és $AuCl_3$ molekulák minimum energiájú szerkezete T-alakú, egy Y-alakú átmeneti állapotú szerkezettel. Az AuI_3 esetében az Y-alakú szerkezet kisebb energiájú, mint a T-alakú. Az $AuBr_3$ és AuI_3 molekulák globális minimuma más; egy L-alakú szerkezet, ami a potenciális-energia felületen a Jahn–Teller felületen kívül esik. Ezt a szerkezetet felfoghatjuk, mint egy donor-akceptor rendszer, vagy mint egy zárt héjú kölcsönhatás, amelyben a I_2 a donor és az AuI az akceptor. Az arany-monohalogenidekben az arany-arany távolság rendkívül rövid, ami az un. aurofil kölcsönhatásra utal. A trihalogenidek dimerjei sík molekulák, két hidas halogén atommal.*

Abstract in German: *Die Molekülstrukturen von allen Gold-Mono- und Trihalogeniden und ihrer Dimere wurde berechnet auf dem B3LYP, MP2, und CCSD(T) Niveau unter Verwendung relativistischer Pseudopotentiale für alle Atome mit Ausnahme vom Fluor. Unsere Rechnungen unterstützen die experimentelle Beobachtung, dass die relative Stabilität der Monohalogenide vom Fluorid zum Iodid größer wird, während der umgekehrte Trend für die Trihalogenide gefunden wird. Die Energiepotentialflächen aller Goldtrihalogenide sind untersucht worden. Diese Moleküle sind typische Jahn–Teller-Systeme; die trigonal-planare D_{3h}-symmetrische Struktur entspricht für keines der untersuchten Trihalogenide der Minimumstruktur. Die Größe und der Charakter der Jahn–Teller-Verzerrung ändert sich graduell vom AuF_3 zum AuI_3. Die Minimumstruktur besitzt eine T-förmige Anordnung der Atome für AuF_3 und $AuCl_3$, während die Y-förmige Anordnung einem Übergangszustand entspricht. Für AuI_3 liegt die Y-förmige Struktur energetisch tiefer auf der Energiepotentialfläche als die T-förmige Struktur. Sowohl für $AuBr_3$ als auch für AuI_3 repräsentiert weder die T- noch die Y-förmige Struktur das globale Minimum sondern eine L-förmige AuX_3 Struktur, welche außerhalb der Jahn–Teller-Fläche liegt. Diese Struktur kann als Donor-Acceptor-System oder closed-shell Wechselwirkung aufgefasst werden, mit I_2 als Donor und AuI als Acceptor. Die Dimere der Goldmonohalogenide besitzen sehr kurze Gold-Gold-Abstände, die auf aurophile Wechselwirkungen hinweisen. Die Dimere der Trihalogenide sind planare Moleküle mit zwei verbrückenden Halogenatomen.*

  0947-6539/01/0717-3658 $ 17.50+.50/0

Experimentally only the monochlorides, -bromides, and -iodides have been known until recently. The existence of AuF was first suggested by computations[21] and then proven by neutralization-reionization mass spectrometric experiments,[22] and finally by microwave spectroscopy,[23] the latter providing the geometry of the molecule as well. Attempts to determine their structure by electron diffraction failed.[24] The molecular constants of AuCl and AuBr have been determined by microwave spectroscopy[25] and for AuCl also from the rotational structure of the visible transitions in the emission spectra.[26] AuF[13, 27, 28, 29] and AuCl[14, 29, 30, 31] have been studied by computations at different levels; for AuBr and AuI only two computational studies have been published.[29, 31] Their dimers have only been studied by computation.[13, 14, 27, 31] There have also been computational studies on isolated anions of gold halides, for example, AuX_2^-, AuX_4^-, AuF_6^-,[15] $AuCl_4^-$,[14] and $Au_2X_4^{2-}$.[32]

The stability of the gold trihalides decreases from the fluorides toward the iodides, and our attempt to register the diffraction picture of the monomer of gold trichloride failed.[14] The chances for an experimental gas-phase structure determination for $AuBr_3$ and AuI_3 are rather slim. According to textbooks, AuI_3 has not even been isolated;[33] it only exists in its complexes as an AuI_4^- ion, although a recent study claimed to have registered a trigonal planar AuI_3 molecule as an inclusion compound in a cluster.[34] $AuBr_3$ and AuI_3 have not yet been studied by computational methods either. The dimers of the trihalides are interesting for their coplanar gold configuration, for example, Au_2F_6 in the vapor phase,[13, 15a] Au_2Cl_6 in the crystal[15a, 35] as well as in the vapor phase,[14, 15a] and Au_2Br_6 in the crystal.[36] This is in accord with the planarity of AuX_4^- ions, but in contrast with most metal trihalide dimers whose geometry is the typical halogen-bridged structure with two distorted tetrahedra sharing a common edge.[37] Gold trifluoride has a helical structure in its crystal with a coplanar gold configuration.[38]

It seems that experimental gas-phase structural determination is not feasible for the complete range of gold halides, and the only techniques for their comprehensive structural study are computational methods. Earlier computations utilized different levels of theory and different basis sets, hence it seemed worthwhile to do a consistent study at the same level of theory and with comparable basis sets. $AuBr_3$ and AuI_3 and their dimers are studied here for the first time.

Computational Details

Our goal was to compare the structures and energetics of all simple gold halide molecules, therefore it was important to carry out the calculations in such a way that the results could be compared reliably with each other. Calculations were carried out with the Gaussian 98 program package.[39] Pseudopotential techniques were applied for all atoms, except fluorine, for which the 6-31G(d) standard basis set was used; the use of all-electron basis sets for first row atoms is better concerning accuracy and efficiency. A multielectron-adjusted quasirelativistic effective core potential covering 60 electrons ($[Kr]4d^{10}4f^{14}$) was used for gold. The halogen pseudopotentials covered the following electronic configurations: Cl: [Ne]; Br: $[Ar]3d^{10}$, and I: $[Kr]4d^{10}$. The basis set for gold was an (8s7p6d)/[6s5p3d]-GTO valence basis set (311111,22111,411). For the halogens a (5s5p1d)/[3s3p1d] valence basis set (311,311,1) was used. Both the pseudopotentials and the corresponding basis sets were those of the Stuttgart group.[40] Comparison of this data set with better basis-set results of Ref. [13] shows differences that were no larger than 0.01 – 0.02 Å for the bond lengths. The reliability of the pseudopotentials for the larger halogens was checked by comparing them with the results of Ref. [14], in which different gold trichlorides were calculated with the same basis/ECPs on Au and several all-electron bases on chlorine. The results were within about 0.02 Å of each other. The bond angles in all these molecules were constant and relatively independent of the basis sets. Trial calculations on the Au_2X_2 dimers at the B3LYP and CCSD(T) level were also carried out with a larger basis set on Au, in which two f-type polarization functions were added, a compact one to describe the Au-X covalent bonds and a diffuse one to describe polarizability and van der Waals interactions (with coefficients 1.19 and 0.2, respectively). These polarization functions did shorten the distances, especially the Au ··· Au distances of the dimers (see Table 1). At the same time, as shown by the data in Table 1, the B3LYP results of this test calculation for Au_2F_2 were not right; in this case the basis set was not balanced, larger basis sets are needed for the fluorine as well to balance the gold basis set. We tried several and at least a 6-31 + G(3d) or better quality is needed. Therefore, to save CPU time, we carried out our further calculations without the additional f functions on gold.

Full geometry optimizations were carried out at three different correlated levels of theory: MP2, density functional with the B3LYP formalism,[41] and CCSD(T). All stationary points were characterized by a frequency analysis at the B3LYP and the MP2 level. Mulliken population analyses and natural bond orbital (NBO) analyses[42] were carried out to investigate the bonding in all molecules at the B3LYP level.

Table 1. Geometries [distances in Å, angles in °].[a]

		F	Cl	Br	I
AuX, $^1\Sigma_g$, $C_{\infty v}$					
Au-X	B3LYP	1.956	2.293	2.406	2.584
	MP2	1.946	2.277	2.389	2.570
	CCSD(T)	1.954	2.293	2.407	2.590
Au_2X_2, ^1A_g, D_{2h}					
Au-X	B3LYP	2.230	2.564	2.659	2.807
	B3LYP (2f)[b]	2.219	2.551	2.646	2.796
	MP2	2.223	2.537	2.631	2.782
	CCSD(T)	2.229	2.557	2.653	2.807
	CCSD(T)(2f)[b]	2.229	2.519	2.613	2.722
Au ··· Au	B3LYP	3.051	2.818	2.809	2.827
	B3LYP (2f)[b]	3.224[c]	2.772	2.761	2.776
	MP2	3.008	2.793	2.776	2.772
	CCSD(T)	2.951	2.797	2.788	2.792
	CCSD(T)(2f)[b]	2.809	2.717	2.708	2.722
∢X-Au-X	B3LYP	93.7	113.3	116.2	119.5
	B3LYP (2f)[b]	86.9	114.2	117.1	120.5
	MP2	94.8	113.2	116.3	120.5
	CCSD(T)	97.1	113.7	116.6	120.4
	CCSD(T)(2f)[b]	101.9	114.9	117.6	121.0
T-shaped AuX_3, $^1A_1$, C_{2v}					
Au1−X2	B3LYP	1.908	2.295	2.434	2.661
	MP2	1.896	2.274	2.413	2.632
	CCSD(T)	1.902	2.287	2.428	2.655
Au1−X3	B3LYP	1.916	2.301	2.432	2.630
	MP2	1.911	2.281	2.408	2.603
	CCSD(T)	1.911	2.293	2.426	2.630
∢X2-Au1-X3	B3LYP	95.0	96.9	97.2	97.8
	MP2	93.9	95.5	96.2	97.5
	CCSD(T)	94.4	95.9	96.2	97.2
Δ[(Au1−X2) – (Au1−X3)]	B3LYP	– 0.008	– 0.006	0.002	0.031
	MP2	– 0.015	– 0.007	0.005	0.029
	CCSD(T)	– 0.009	– 0.006	0.002	0.025

Table 1. Continued

		F	Cl	Br	I
Y-shaped AuX_3, $^1A_1$, C_{2v}					
Au1−X2	B3LYP	1.919	2.287	2.411	2.603
	MP2	1.909	2.254	2.375	2.569
	CCSD(T)	1.916	2.276	2.401	2.598
Au1−X3	B3LYP	1.909	2.310	2.450	2.688
	MP2	1.902	2.291	2.425	2.631
	CCSD(T)	1.903	2.301	2.444	2.671
∢X2-Au1-X3	B3LYP	139.6	137.9	138.6	141.9
	MP2	140.0	138.5	138.4	138.5
	CCSD(T)	139.6	138.2	138.6	140.1
Δ[(Au1−X2) − (Au1−X3)]	B3LYP	0.010	− 0.023	− 0.039	− 0.085
	MP2	0.007	− 0.037	− 0.050	− 0.062
	CCSD(T)	0.013	− 0.025	− 0.043	− 0.073
L-shaped AuX_3, $^1A'$, C_s[d]					
Au1−X2	B3LYP	1.912	2.275	2.398	2.588
	MP2	1.925	2.259	2.380	2.571
	CCSD(T)		2.277	2.400	2.593
Au1−X3	B3LYP	2.003	2.360	2.475	2.666
	MP2	2.237	2.381	2.474	2.654
	CCSD(T)		2.400	2.500	2.684
Au1−X4	B3LYP	3.093	3.748	3.991	4.394
	MP2	3.032	3.595	3.812	4.169
	CCSD(T)	–	3.635	3.857	4.221
X3−X4	B3LYP	1.572	2.125	2.382	2.786
	MP2	1.444	2.063	2.331	2.744
	CCSD(T)	–	2.094	2.363	2.779
∢X2-Au1-X3	B3LYP	167.3	171.6	172.6	173.9
	MP2	174.8	175.7	176.1	177.3
	CCSD(T)	–	175.4	176.0	177.3
∢Au1-X3-X4	B3LYP	119.3	113.3	110.5	107.4
	MP2	109.0	107.8	105.0	101.1
	CCSD(T)		107.8	105.0	101.2
Au_2X_6, ^1A_g, D_{2h}					
Au1−X5	B3LYP	1.896	2.307	2.452	2.677
	MP2	1.889	2.286	2.433	2.659
	CCSD(T)	1.891	2.296	2.445	2.677
Au1−X3	B3LYP	2.062	2.437	2.566	2.763
	MP2	2.052	2.403	2.526	2.719
	CCSD(T)	2.052	2.422	2.550	2.751
Au1 ··· Au2	B3LYP	3.187	3.586	3.747	4.040
	MP2	3.147	3.495	3.649	3.942
	CCSD(T)	3.164	3.766	3.844	3.994
∢X3-Au1-X4	B3LYP	78.8	85.3	86.2	86.0
	MP2	79.8	86.7	87.5	87.1
	CCSD(T)	79.1	86.4	87.4	87.1
∢X5-Au1-X6	B3LYP	89.7	90.9	91.1	91.5
	MP2	89.3	90.4	90.7	91.8
	CCSD(T)	89.6	90.6	90.5	90.8
X_2, $^1\Sigma_g$, $D_{\infty h}$					
X1−X2	B3LYP	1.404	2.059	2.323	2.734
	MP2	1.421	2.043	2.310	2.728
	CCSD(T)	1.444	2.067	2.337	2.760

[a] Experimental geometries: AuF:[23] r_e(Au−F) = 1.918449(5) Å; AuCl: Au−Cl = 2.1990287(9) Å,[25], 2.19903(21) Å;[26] AuBr:[25] Au−Br = 2.318410(1) Å; AuF_3:[13] r_g(Au1−F2) = 1.893(12) Å, r_g(Au1−F3) = 1.913(8) Å, $\sphericalangle_a$F2-Au1-F3 = 102.5(1.9)°; Au_2F_6 (at 600 K):[13] r_g(Au1−F5) = 1.876(6) Å, r_g(Au1−F3) = 2.033(7) Å, $\sphericalangle_a$F3-Au1-F4 = 80.4(1.6)°, $\sphericalangle_a$F5-Au1-F6 = 92.1(1.0)°; Au_2Cl_6:[14] r_g(Au1−Cl5) = 2.236(13) Å, r_g(Au1−Cl3) = 2.355(13) Å, $\sphericalangle_a$Cl3-Au1-Cl4 = 86.8(1.8)°, $\sphericalangle_a$Cl5-Au1-Cl6 = 92.7(2.5)°. [b] Calculation with two additional f-type polarization functions on Au, see text. [c] r(Au ··· Au) = 2.969 Å with a 6-31 + G(3d) basis set on fluorine. [d] Always *trans* geometry.

Our earlier results indicated that both AuF_3 and $AuCl_3$ are Jahn–Teller distorted molecules with a typical "Mexican hat" type potential energy surface (PES).[13, 14] This time the PES of $AuBr_3$ and AuI_3 was calculated at the B3LYP level. For comparison the PESs of AuF_3 and $AuCl_3$ are also shown, in these last two cases the full electron aug-cc-pVDZ basis sets were used for the halogens. In each case the energy was calculated as a function of the two X-Au-X angles in 5° steps. None of the determined points was corrected for zero-point vibrations; such corrections are calculated to be rather small, of the order of 0.1–0.2 kcal mol^{-1}, in the harmonic approximation.

Intrinsic reaction coordinate (IRC) calculations were carried out to check whether the located transition states belong to either of the two minima under consideration. 200 points in both directions were calculated. In cases in which 200 steps did not lead to a minimum, an optimization followed that utilized the last geometry of the IRC.

The computed geometrical parameters for all molecules are given in Table 1 and the relative energies in Table 2. The computed frequencies and absolute energies are given as Supporting Information. Molecular models and the numbering of atoms in all species are shown in Figure 1. In our discussion, unless otherwise noted, CCSD(T) geometries and energies will be quoted.

Results and Discussion

Gold monohalide monomers: The stability of gold monohalides increases from the fluorides towards the iodides; thus while AuI is a well-known solid with a zig-zag chain-like structure and two-coordinate gold,[43] the very existence of AuF has only been proven recently (vide supra).[21, 22] Its Au−F bond length (r_e) is 1.918449(5) Å, from microwave spectroscopy.[23] From among the many computed values, the 1.922 Å (MP2) value of Schwerdtfeger et al.[27] is the closest to the experimental bond length, followed by our earlier MP2/F: aug-cc-PVTZ value of 1.911 Å. The bond lengths from higher level computations, such as CCSD(T) and QCISD(T) tend to be a few hundredths of an angstrom larger. The experimental bond lengths of AuCl and AuBr (2.1990287(9)[25] and 2.318410(1) Å,[25] respectively) are shorter than the computed values by almost 0.1 Å. There is one consistent set of MP2-level bond lengths for the AuX and Au_2X_2 systems (X = Cl, Br, I) in the literature,[31] in good agreement with our results.

Gold fluoride (AuF) is the best-studied binary gold-halide so far, especially by Schwerdtfeger and co-workers.[21, 27, 29, 30] These and other studies[28] have been mostly concerned about the role of relativistic and correlation effects on the geometry and other properties of these systems. The shortening of bonds due to relativistic effects is especially pronounced in the monohalides of gold as the 0.184 Å (MP2)/0.175 Å (CCSD(T)) and the 0.192 Å (CCSD(T)) decreases demonstrate (these values were calculated for AuF[27] and AuCl,[30] respectively). This is due to the pronounced contraction of the 6s orbital in the d^{10} electronic configuration of gold.

Comparison of the bond lengths of the monohalides with those of the trihalides (vide infra) shows a changing pattern. We would expect the monohalides to have longer bonds than the trihalides and this is observed for the fluorides; the Au−F bond is about 0.05 Å longer than the

0947-6539/01/0717-3660 $ 17.50+.50/0 *Chem. Eur. J.* **2001**, *7*, No. 17

Table 2. Relative energies [kcal mol^{-1}].[a]

	ΔE_0				ΔH_{298}				ΔG_{298}			
	F	Cl	Br	I	F	Cl	Br	I	F	Cl	Br	I
T-AuX$_3$ → Y-AuX$_3$												
B3LYP	4.72	2.52	1.30	– 1.20	4.12	1.92	0.70	– 0.62	5.27	3.33	2.47	– 2.81
MP2	5.75	2.58	1.29	– 0.08	5.16	1.98	0.70	– 0.08	6.13	3.28	2.37	– 0.01
CCSD(T)[b]	5.65	2.95	1.52	– 0.67	5.07	2.35	0.93	– 0.67	6.04	3.65	2.60	– 0.60
T-AuX$_3$ → L-AuX$_3$												
B3LYP	49.65	3.10	– 3.18	– 7.42	45.20	1.16	– 3.89	– 6.21	43.15	– 1.11	– 6.16	– 6.55
MP2	67.39	12.33	5.61	0.06	62.08	10.38	4.91	0.73	59.57	8.28	2.64	– 1.85
CCSD(T)[b]	–	6.91	– 0.06	– 5.11	–	4.96	– 0.75	– 4.44	–	2.86	– 3.03	– 7.02
T-AuX$_3$ → AuX + X$_2$												
B3LYP	67.87	20.18	16.43	13.14	67.23	19.56	15.81	13.12	58.22	10.96	7.51	3.10
MP2	76.25	30.36	27.24	23.77	75.49	29.73	26.61	23.73	66.21	20.89	18.01	13.54
CCSD(T)[b]	68.04	24.37	20.67	17.36	67.28	23.73	20.03	17.32	58.00	14.89	11.44	7.13
Y-AuX$_3$ → AuX + X$_2$												
B3LYP	63.15	17.66	15.13	14.34	63.11	17.64	15.11	13.74	52.95	7.62	5.04	5.91
MP2	70.50	27.78	25.95	23.85	70.33	27.75	25.91	23.81	60.08	17.60	15.64	13.55
CCSD(T)[b]	62.39	21.42	19.15	18.03	62.21	21.39	19.11	17.99	51.96	11.24	8.84	7.73
L-AuX$_3$ → AuX + X$_2$												
B3LYP	18.22	17.08	19.61	20.56	17.92	16.49	19.00	19.95	9.80	8.74	11.20	12.46
MP2	8.86	18.03	21.63	23.70	8.25	17.38	21.00	23.08	0.51	9.32	13.01	15.40
CCSD(T)[b]	–	17.46	20.73	22.47	–	16.80	20.09	21.85	–	8.75	12.10	14.17
2 T-AuX$_3$ → Au$_2$X$_6$												
B3LYP	– 70.74	– 46.90	– 43.66	– 37.46	– 69.22	– 45.57	– 42.41	– 35.06	– 54.84	– 31.65	– 28.51	– 25.46
MP2	– 77.90	– 62.39	– 60.91	– 56.84	– 76.39	– 61.04	– 59.65	– 54.43	– 62.82	– 47.55	– 45.88	– 44.31
CCSD(T)[b]	– 77.36	– 57.82	– 54.66	– 48.19	– 75.85	– 56.48	– 53.40	– 45.78	– 62.28	– 42.99	– 39.63	– 35.66
2 AuX → Au$_2$X$_2$												
B3LYP	– 16.93	– 20.71	– 23.74	– 28.08	– 16.57	– 20.19	– 23.18	– 27.50	– 8.25	– 11.34	– 14.68	– 18.64
MP2	– 24.19	– 29.22	– 33.15	– 38.99	– 23.84	– 28.72	– 32.59	– 38.40	– 15.14	– 19.77	– 23.85	– 29.35
CCSD(T)[b]	– 24.35	– 29.66	– 33.14	– 38.26	– 24.00	– 29.15	– 32.58	– 37.67	– 15.30	– 20.20	– 23.84	– 28.62
Au$_2$X$_6$ → Au$_2$X$_2$ + 2 X$_2$												
B3LYP	189.56	66.54	52.77	35.67	187.11	64.49	50.84	33.80	163.03	42.23	28.85	13.02
MP2	206.21	93.89	82.24	65.39	203.53	91.78	80.27	63.49	180.10	69.55	58.05	42.03
CCSD(T)[b]	189.10	76.91	62.86	44.65	186.41	74.80	60.89	42.75	162.99	52.57	38.67	21.30

[a] Basis-set superposition error was not calculated, since we found no obvious ways to do the counterpoise calculation for these systems. [b] The temperature correction was taken from the MP2 calculation, since no CCSD(T) frequencies were available; for L-shaped AuF_3 the CCSD(T) method did not converge.

shorter bond of the T-shaped ground-state structure of AuF_3 (our earlier higher level computation gave a difference of 0.06 Å).[13] For the chlorides the bond lengths are about the same in the two molecules, while for the bromides and especially the iodides the trend reverses and the trihalides have longer bonds. This is in accord with the fact that the stability of monohalides increases towards the iodides while the opposite is true for the trihalides; hence the bonds get gradually longer/weaker in the trihalides. Another possible explanation is the different extent of relativistic shortening of bonds in the mono- and trihalides. While the relativistic shortening of the monohalides is large, due to the substantial contraction of the 6s orbital (vide supra), it is much less pronounced for the trihalides, for which the expansion of the 5d orbitals partially compensates the contraction of the 6s orbitals. The increasing relativistic shortening of the heavier monohalides compared with the lighter ones increases their stability and makes their bonds eventually shorter compared with the trihalides. For the trihalides, the larger degree of ionic bonding in AuF_3, compared with the heavier trihalides, stabilizes its higher oxidation state. At the same time, the larger relativistic effects in the heavier halides increase the gap between the s and p orbitals, making the p orbitals less available for bonding and, therefore, being at least partially responsible for their decreasing stability.

Gold trihalide monomers: The usual D_{3h} symmetry trigonal planar arrangement of metal trihalides is not a minimum structure for either of these gold trihalides. These molecules, with gold in a formal d^8 electronic configuration, are subjected to Jahn–Teller distortions, and this is confirmed by this study for all four molecules, in accord with earlier experimental evidence for AuF_3[13] and with computations for both AuF_3[13, 15] and $AuCl_3$[14, 15] (molecular models and the numbering of atoms in all species studied are shown in Figure 1). The amount and character of the Jahn–Teller distortion, however,

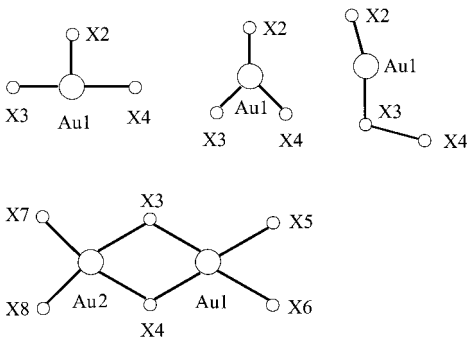

Figure 1. Molecular models and numbering of atoms in T-, Y-, and L-shaped AuX_3, and in Au_2X_6.

is different in the four trihalides; they change gradually from the trifluoride to the triiodide.

We have calculated the PES of all four molecules at the B3LYP level, see Figure 2. The Jahn–Teller surface is a typical "Mexican hat" potential energy surface for gold trifluoride[13] and trichloride,[14] indicative of Jahn–Teller distortions for which the quadratic coupling terms are of importance in describing the vibronic interaction (vide infra).[7] For all four molecules the Jahn–Teller surface has two types of low-energy structures; a T-shaped and a Y-shaped structure (see Figures 1 and 2). The T-shaped structure is the minimum of the Jahn–Teller surface for the first three trihalides, and for AuF_3 and $AuCl_3$ it corresponds to the global minimum of the ground-state molecule. The Y-shaped geometry for these molecules describes the transition state between two minima by way of the exchange of the positions of the X2 and X3 or X4 atoms. The Jahn–Teller stabilization energy (the difference between the D_{3h}-symmetry singlet ($^1E'$), trigonal planar structure, and the minimum-energy structure on the Jahn–Teller surface) is about 29.4, 17.8, 15.5, and 14.0 kcal mol^{-1} for AuF_3, $AuCl_3$, $AuBr_3$, and AuI_3, respectively, at the B3LYP level. The energy difference between the minimum energy structure and the triplet, $^3E'$, trigonal planar geometry is smaller and also decreases, 12.8, 6.6, 5.2, and 4.8 kcal mol^{-1}, for the above trihalides (B3LYP). Therefore, for $AuBr_3$ and AuI_3 the energy gain due to the Jahn–Teller distortion is not very large; hence both species possess a very flat potential energy surface (Figure 2 bottom).

The energy difference between the T- and Y-shaped structures also decreases, 4.7, 2.5, 1.3, and -1.2 kcal mol^{-1} at the B3LYP, and 5.7, 3.0, 1.5, and -0.7 kcal mol^{-1} at the CCSD(T) level for AuF_3, $AuCl_3$, $AuBr_3$, and AuI_3, respectively. For AuI_3 the Y-shaped structure is somewhat lower in energy than the T-shaped structure, and even that does not appear to be a true minimum but a transition state at the MP2 level (although minimum at the B3LYP level). Thus, we found it of importance to check the PES of AuX_3 further, beyond the Jahn–Teller surface. It appears that, indeed, there is a much lower energy structure with C_s symmetry (see Figures 1 and 2, vide supra) for $AuBr_3$ and AuI_3 with a direct X–X bond (vide infra).

Due to the gradual decrease of the energy difference between the T- and Y-shaped structures, the four molecules can perhaps be classified into two groups. AuF_3 and $AuCl_3$ can be considered as ideal examples of static Jahn–Teller systems, for which the energy difference between the local minima and saddle points on the brim of the PES are large enough to prevent the molecule to pseudorotate, and thus the molecule is locked in the nondegenerate, distorted minimum positions. The splitting of the peak corresponding to the nonbonded distances of AuF_3 on the electron-diffraction radial distribution curve provides evidence for this (vide supra).[13] The energy difference of about 5 kcal mol^{-1} is large enough to keep the molecules at the minima and for the molecules to have the T-shaped structure in the gas phase even at the 1100 K temperature of the electron diffraction experiment. Although our attempts to record electron diffraction patterns for the monomeric $AuCl_3$ failed, the energy difference is high enough to classify the molecule as a static Jahn–Teller case.

In contrast, the energy difference between the T- and Y-shaped structures for both $AuBr_3$ and AuI_3 is very small so the molecules can be considered more as a dynamic Jahn–Teller system. The frequency associated with the exchange of the halogen atoms between the T- and Y-shaped structures is very small; this makes the calculations sensitive to changes in the applied method, basis set, etc. We may have reached the limit for frequency analysis here, although all three

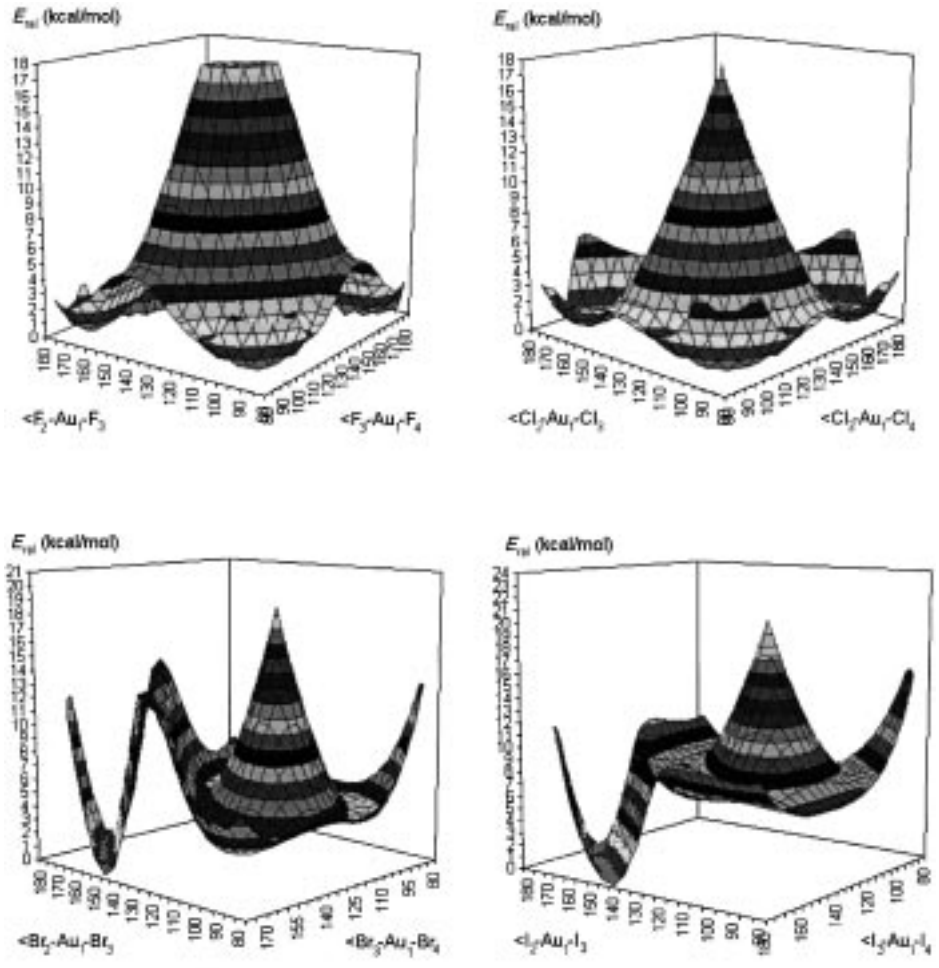

Figure 2. Potential energy surfaces of all AuX_3 molecules at the B3LYP level (for applied basis sets see text). (See also refs. [13] and [14]).

0947-6539/01/0717-3662 $ 17.50+.50/0 *Chem. Eur. J.* **2001**, *7*, No. 17

methods used here (B3LYP, MP2, and CCSD(T)) agree on the relative stabilities of the T- and Y-shaped structures, offering some confidence in the results.

Relativistic effects enhance the Jahn–Teller distortions in all AuX_3 molecules. They lower the energy of the Au 6s orbital and increase the energy of the 5d orbital. Thus the 5d orbitals become major contributors to the valence shell and their shape favors a larger angular distortion. The Jahn–Teller distortion is largest in AuF_3 and decreases along the series as pronounced both in the bond lengths and the bond angles. This is the consequence of the large contraction of the Au 6s orbital; in spite of the large size of Au, energetically it will be closest to the fluorine orbitals and thus will have the largest overlap with them. Figure 3 illustrates this with two selected sigma bonding MOs of the same symmetry; the decreasing overlap as going from the fluoride towards the iodide is conspicuous.

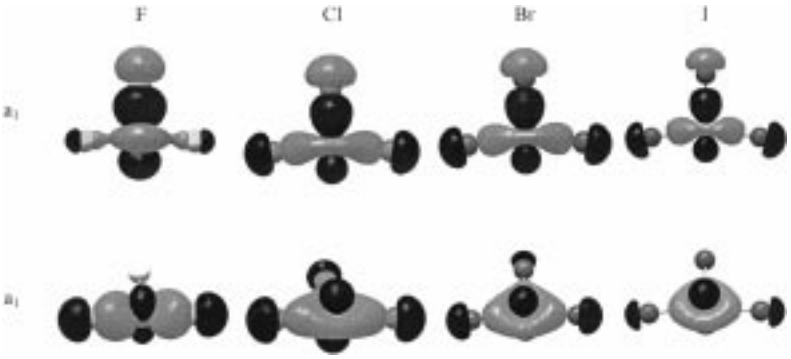

Figure 3. Molecular orbitals showing sigma-type bonding in T-shaped AuX_3 (HF orbitals at the MP2 geometry).

The decreasing amount of distortion along the series is also reflected by their MO schemes. The splitting of the e-type orbitals of the D_{3h}-symmetry structure is largest for AuF_3 and the orbital gaps decrease down the group among the halogens (Table 3).

T-shaped structure: This structure has one shorter and two longer Au–X bonds, and two smaller and one larger X-Au-X bond angles in AuF_3 and $AuCl_3$ (Figure 1). The difference between the two types of Au–X bonds, $\Delta[(Au1–X2) – (Au1–X3)]$, changes from -0.009 Å in the trifluoride to -0.006 Å in the trichloride. Although the T-shaped structure is still a minimum structure for $AuBr_3$ at all levels considered, the character of this structure changes: there is one longer and two shorter Au–Br bonds with a difference of 0.002 Å between them.

AuI_3 is different, for this molecule the T-shaped structure is no longer the minimum of the Jahn–Teller surface; it has one imaginary frequency and corresponds to a transition state. The relationship of the three bond lengths is similar to that in $AuBr_3$; there are one longer and two shorter bonds with a difference of 0.025 Å between them. Thus, the difference of the two types of bond lengths, $\Delta[(Au1–X2) – (Au1–X3)]$, changes gradually from AuF_3 to AuI_3 as -0.009, -0.006, 0.002, and 0.025, respectively.

The bond angles of the T-shaped structure also show a gradual change from AuF_3 to AuI_3; the X2-Au1-X3 angle is smallest in AuF_3 (94.4°) and largest in AuI_3 (97.2°), in accord with the decreasing degree of Jahn–Teller distortion along the series. It can also be explained by the increasing nonbonded interactions. The F2···F3 distance in AuF_3 is similar to the 1,3-nonbonded F···F distances in other molecules. For $AuCl_3$ this nonbonded distance is already shorter than the average of such distances determined for other molecules, especially if we consider molecules with similarly large central atoms. This effect is even larger for the tribromide and the triiodide, so the observed increase of the X2-Au1-X3 angle is not surprising.

Y-shaped structure: This structure corresponds to a transition state for AuF_3, $AuCl_3$, and $AuBr_3$, with one imaginary frequency (see Supporting Information). The energy barrier associated with this imaginary frequency is largest for AuF_3 (5.7 kcal mol^{-1}), and gradually decreases for $AuCl_3$, (3.0 kcal mol^{-1}) and $AuBr_3$ (1.5 kcal mol^{-1}). Finally, this structure becomes the minimum on the Jahn–Teller surface for AuI_3, being 0.7 kcal mol^{-1} lower in energy than the T-shaped structure. Similarly to the T-shaped geometries, gradual changes are observed in the actual geometrical parameters of the Y-shaped structures as well. The difference between the two types of Au–X bonds, $\Delta[(Au1–X2) – (Au1–X3)]$, varies as X = F: 0.013, Cl: -0.025, Br: -0.043, and I: -0.072 Å. Thus, for AuF_3, the Y-shaped structure has one longer and two shorter bonds and two larger and one smaller bond angles (see, Figure 1). This type of relationship between the geometrical parameters of the Y-shaped and T-shaped molecules can be expected, considering the opposite phases of the Jahn–Teller active vibration and it is also observed, for example, in MnF_3.[12] $AuCl_3$ is different; it has one short and two longer bonds in its Y-shaped geometry, while the relationship of the bond angles is the same as for AuF_3. Thus, for $AuCl_3$, both the T-shaped

Table 3. Orbital energies [au][a] and energy gaps [kcal mol^{-1}] due to Jahn–Teller distortion of T-shaped AuX_3, $e'' \Rightarrow b_1 – a_2$ and $e' \Rightarrow b_2 – a_1$.

	b_1	a_2	gap($a_2 – b_1$)	b_2	a_1(virt.)	gap($a_1 – b_2$)	gap($a_2 – b_2$)
F	–0.60733	–0.56547	26.30	–0.56647	–0.10506	289.50	0.63
Cl	–0.47426	–0.45097	14.61	–0.44751	–0.13248	197.68	–2.17
Br	–0.43117	–0.41228	11.85	–0.40359	–0.13293	169.84	–5.45
I	–0.37976	–0.36577	8.78	–0.35120	–0.13180	137.67	–9.14

[a] HF orbital energies at the CCSD(T) geometry.

  0947-6539/01/0717-3663 $ 17.50+.50/0

ground state and the Y-shaped transition-state structures have one shorter and two longer bonds. This has been interpreted earlier[14] by the very short Cl3···Cl4 distance in the Y-shaped molecule. Using the present levels of calculation and comparing with the computed 1,3 X···X distances in other halides with large central atoms,[37] the X3···X4 distances are about 0.6, 0.8, and 1.0 Å shorter in the AuX_3 (X = Cl, Br, I) Y-shaped structures, respectively. These are very large differences and they explain why the stability of these species with respect to decomposition into AuX and X_2 decreases towards the heavier halides (Tables 1 and 2). Another possible reason for these differences in the geometries is the relative role of the true Jahn–Teller effect and the possible pseudo-Jahn–Teller effect[44] in these molecules. It has been suggested that pseudo-Jahn–Teller effects can happen with molecules with D_{3h} symmetry in which the $^1A_1$ and $^1E'$ states often get close in energy.[18, 45] E × e Jahn–Teller cases are typical examples of having both true and pseudo-Jahn–Teller effects; their relative magnitudes depend on the energy differences of the two states.

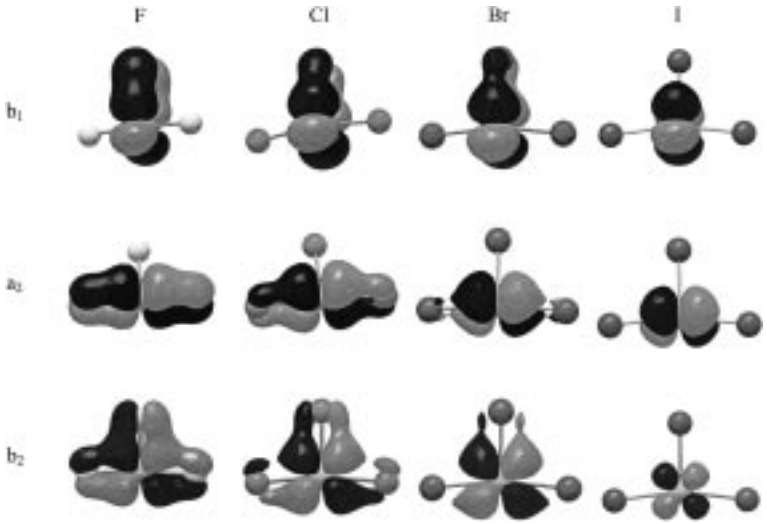

Figure 4. Molecular orbitals showing π back-bonding in T-shaped AuX_3 (HF orbitals at the MP2 geometry).

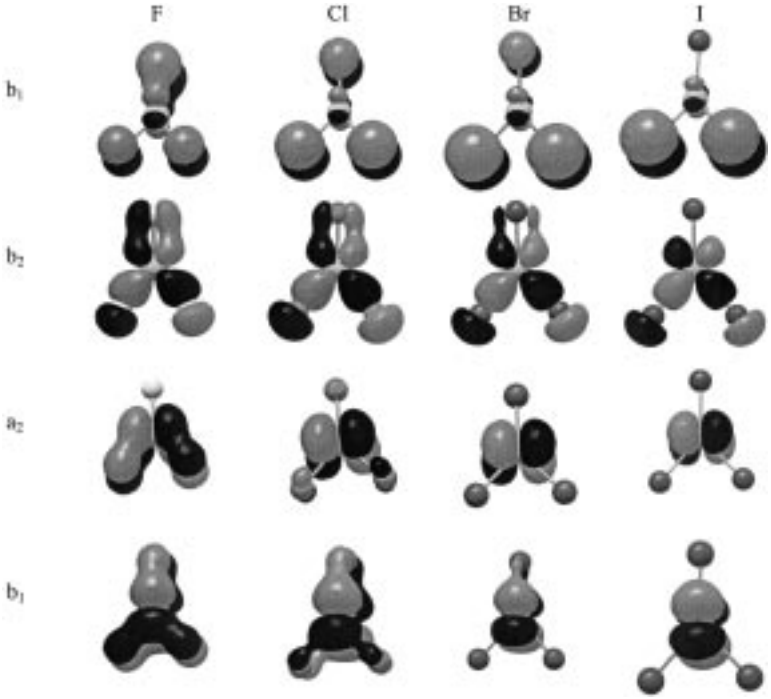

Figure 5. Molecular orbitals showing π back-bonding in Y-shaped AuX_3 (HF orbitals at the MP2 geometry).

Bonding in T- and Y-shaped gold trihalides: An interesting feature of these molecules is their π bonding. It has been shown[14] that there is a considerable π back-bonding in the T-shaped structure of both AuF_3 and $AuCl_3$. Figure 4 shows the relevant MOs for all four molecules. There are three bonding π MOs with b_1, a_2 (both out-of-plane), and b_2 (in-plane) symmetry. The a_2 MOs are 3-center bonds, whereas the b_2 MO is delocalized over the entire molecule. As seen from the figure, the π bonding decreases gradually from the trifluoride to the triiodide. In AuI_3 there is almost no π overlap. This is also in accordance with the decreasing stability of the gold trihalides going from AuF_3 to AuI_3. There is also a certain amount of π bonding in the Y-shaped structures (Figure 5), but that decreases even faster than that in the T-shaped molecules from AuF_3 to AuI_3. Again, for AuI_3 there is almost no π bonding. For the Au–X3 and Au–X4 bonds the π bond is present only in AuF_3, and this may be one of the reasons why the relative lengths of the Au1–X2 versus Au1–X3,4 bonds changes; while Au1–X2 is longer and the other two are shorter in AuF_3, this reverses in $AuCl_3$ and the rest of the molecules. The difference between the two types of bonds increases as the halogen size increases; this is also in accord with the weakening of the Au1–X3,4 bonds and the instability of these molecules against decomposition into AuX and X_2.

An interesting feature of the Y-shaped molecules is their X···X interaction. Figure 6 shows the relevant MOs. Comparing the $1a_1$ orbitals in the four molecules, in AuF_3 the fluorine p-type AOs do not overlap with each other, rather, they participate in a 3-center Au-F bond. The same applies for $AuCl_3$, although with a small amount of Au1–X2 overlap mixing in. For $AuBr_3$ and AuI_3 the p atomic orbitals (AOs) of

0947-6539/01/0717-3664 $ 17.50+.50/0 *Chem. Eur. J.* **2001**, *7*, No. 17

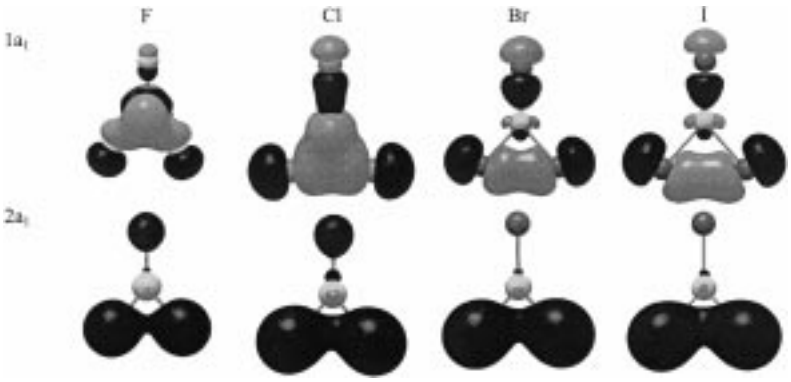

Figure 6. X···X interaction in Y-shaped AuX_3 (HF orbitals at the MP2 geometry).

the X3 and X4 halogens overlap with each other, providing a direct X···X interaction. There is no more interaction between these halogens and the Au atom, while the overlap between the Au and the third halogen is still there. The direct interaction between the halogens is evident for all four molecules in case of the $2a_1$ MO (Figure 6).

The natural bond orbital (NBO) partial charges for both T- and Y-shaped structures are given in Table 4. AuF_3 is a highly polarized molecule, with the halogen charge being somewhat smaller on the X2 atom than on the X3,4 atoms for the T-shaped structure and vice versa for the Y-shaped structure. The polarization decreases the heavier the halogen. The charges on all atoms decrease from the trifluoride to the triiodide. The results of the population analysis are also given in Table 4 for all four molecules. They show that the population of the 6p orbitals is small and, hence, they are *not* included in the Au–X interaction; only 5d and 6s Au orbitals participate in the bond formation. In accord with decreasing π back-bonding and decreasing polarization, the 6s and 5d populations increase in the order F < Cl < Br < I, especially for the Y-species. Both partial charge and natural electron population considerations indicate that assuming formal d^8 Au^{3+} ions to be present in these trihalides is not correct.

L-shaped structures: In view of the flat Jahn–Teller surface of $AuBr_3$ and AuI_3, we further explored the potential energy surfaces of these molecules. It appears that there is, indeed, another low-energy structure, deeper than the minima of the Jahn–Teller surface by about 3 and 7 kcal mol^{-1} for $AuBr_3$ and AuI_3, respectively (see Figure 2 bottom and Table 2, B3LYP). The CCSD(T) method yields 5 kcal mol^{-1} lower

Table 4. Results of NBO analysis for AuX, AuX_3, and their dimers [q in e].

AuX	q(Au)	q(X)			BO(Au–X)	Natural electron configuration
F	0.5273	–0.5273			0.4737	[core]6s(0.66)5d(9.74)6p(0.05)
Cl	0.5040	–0.5040			0.4853	[core]6s(0.61)5d(9.86)6p(0.02)
Br	0.4383	–0.4383			0.5471	[core]6s(0.66)5d(9.88)6p(0.02)
I	0.3386	–0.3386			0.6420	[core]6s(0.73)5d(9.91)6p(0.02)
T-shaped AuX_3	q(Au)	q(X2)	q(X3/4)	q(X3/4) – q(X2)		Natural electron configuration
F	1.4383	–0.3784	–0.5300	–0.1516		[core]6s(0.51)5d(8.96)6p(0.09)
Cl	0.9689	–0.1871	–0.3909	–0.2038		[core]6s(0.62)5d(9.36)6p(0.04)
Br	0.7846	–0.1282	–0.3282	–0.2000		[core]6s(0.69)5d(9.47)6p(0.05)
I	0.5433	–0.0599	–0.2417	–0.1818		[core]6s(0.79)5d(9.60)6p(0.06)
Y-shaped AuX_3	q(Au)	q(X2)	q(X3/4)	q(X3/4) – q(X2)		Natural electron configuration
F	1.3458	–0.5140	–0.4159	0.0981		[core]6s(0.67)5d(8.90)6p(0.08)
Cl	0.9163	–0.4113	–0.2525	0.1588		[core]6s(0.68)5d(9.35)6p(0.04)
Br	0.7375	–0.3544	–0.1915	0.1629		[core]6s(0.73)5d(9.47)6p(0.04)
I	0.4934	–0.2825	–0.1054	0.1771		[core]6s(0.81)5d(9.63)6p(0.05)
L-shaped AuX_3	q(Au)	q(X2)	q(X3)	q(X4)		Natural electron configuration
F	0.5642	–0.5359	–0.0491	0.0208		[core]6s(0.78)5d(9.60)6p(0.07)
Cl	0.4680	–0.5173	0.0336	0.0157		[core]6s(0.78)5d(9.72)6p(0.02)
Br	0.3886	–0.4660	0.0638	0.0137		[core]6s(0.81)5d(9.76)7p(0.03)
I	0.2706	–0.3971	0.1052	0.0213		[core]6s(0.87)5d(9.82)6p(0.03)
Au_2X_2	q(Au)	q(X)			BO(Au···Au)	Natural electron configuration
F	0.6500	–0.6500			0.0477	[core]6s(0.36)5d(9.92)6p(0.08)
Cl	0.6205	–0.6205			0.0697	[core]6s(0.43)5d(9.92)6p(0.02)
Br	0.5375	–0.5375			0.0814	[core]6s(0.50)5d(9.92)6p(0.03)
I	0.4139	–0.4139			0.0939	[core]6s(0.61)5d(9.93)6p(0.03)
Au_2X_6	q(Au)	q(X3)	q(X5)	q(X3) – q(X5)		Natural electron configuration
F	1.4497	–0.5427	–0.4535	–0.0892		[core]6s(0.56)5d(8.91)6p(0.07)
Cl	0.9417	–0.3162	–0.3128	0.0034		[core]6s(0.64)5d(9.36)6p(0.04)
Br	0.7602	–0.2243	–0.2680	0.0437		[core]6s(0.70)5d(9.47)6p(0.04)
I	0.5216	–0.1000	–0.2108	0.1108		[core]6s(0.80)5d(9.60)6p(0.05)

energy for L-shaped AuI_3 and about the same energy for the L- and T-shaped $AuBr_3$. Apparently, the heavier the halogen the more stable this L-shaped structure becomes by all computational methods; frequency analyses show that this structure is a true minimum for all AuX_3 molecules. This L-shaped structure has C_S symmetry, as shown in Figure 1. The L-shaped $AuCl_3$ is estimated to be about 3 kcal mol^{-1} higher in energy than the T-shaped minimum by the B3LYP method (7 kcal mol^{-1} by CCSD(T)). At the same time this structure is about 50 kcal mol^{-1} higher in energy than the T-shaped minimum for AuF_3 (B3LYP, the coupled cluster calculation for AuF_3 did not converge.)

To gain further insight into the isomerization of the C_{2v}-symmetry (T- and Y-shape) structures to the L-shaped C_s-symmetry structure, we have located the transition states of the reaction paths: i) T-shaped → L-shaped for AuX_3, X = F, Cl and Br, and ii) Y-shaped → L-shaped for AuI_3. The geometrical parameters of the transition-state structures are given as Supporting Information. The activation barrier is calculated to be very large (58 kcal mol^{-1}) for AuF_3, dramatically decreasing to 18 ($AuCl_3$), 8 ($AuBr_3$), and 2 kcal mol^{-1} (AuI_3) for the heavier halogen species. Several factors contribute to the activation barrier for this type of halogen shift: i) unfavorable charge distribution (electrostatic repulsion between X3 and X4 atoms, cf. Table 4); ii) breaking of the Au1–X4 bond; iii) charge redistribution upon making the X3–X4 bond.[46] The large electrostatic repulsion, together with the small F_2 bond energy, as compared with, for example, Cl_2, explains the large barrier for AuF_3. It should be noted that polar solvents or lattice effects may have a considerable influence on the activation barrier. AuI_3 should be the best candidate to find the C_s structure in an experiment, because of the very small activation barrier to overcome. Once the C_s-symmetrical AuI_3 is formed, it should be fairly stable as the activation barrier in the other direction is larger, about 8 kcal mol^{-1}. If we consider the reaction AuI + I_2 → L-AuI_3, the formation of the L-shaped molecule happens without an activation barrier in an exothermic reaction.

The L-shaped AuX_3 molecule has only two Au–X bonds and one direct X–X interaction. Since experimentally AuI_3 seems to be the most relevant, our discussion focuses on that molecule. The Au1–I2 bond is about the same as in the Y-shaped structure (which is the lower energy structure on the Jahn–Teller surface of AuI_3), and the Au1–I3 bond is only 0.013 Å longer than the corresponding bond in the Y-shaped molecule. The third gold–iodine bond of the C_{2v}-symmetrical trihalide disappears here. The Au1···I4 distance, with its 4.221 Å length, of course, is no longer a bond; it is even longer than the I···I van der Waals interaction (3.96 Å). At the same time, the I3···I4 distance is 2.779 Å, which is only 0.019 Å longer than the bond in the iodine molecule calculated by the same method, 2.760 Å.

Bonding in L-shaped gold trihalides: This rather intriguing structure can be rationalized by qualitative valence bond (VB) considerations. Figure 7 shows three different types of canonical Lewis structures (**A**–**C**) possible for this molecule. In each of these structures the gold atom has an expanded valence shell in which the 5d electrons are also taken into consideration.

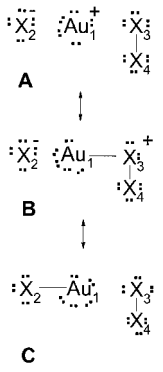

Figure 7. Canonical Lewis structures of L-shaped AuX_3.

In the NBO analysis that we carried out for all molecules, two-center bonds and lone pairs are localized, and only one sigma bond between Au and X2 and one sigma bond between X3 and X4 are considered. Hence, the NBO Lewis picture corresponds to structure **C** (Figure 7). This structure describes the molecule as consisting of two separate, closed-shell fragments, AuX and X_2. This is indicated, for example, by the partial charges. For the gold atom as well as for the X2 atom of the L-shaped trihalides, the partial charges are almost the same as in the corresponding monohalides (see, Table 4). On Au they change from +0.56 in AuF_3 to +0.27 in AuI_3, an indication of an increasing covalent character for the heavier halides. For all species the partial charges of the X–X unit are almost zero ($\leq$0.1) indicating that the Lewis structure **C** is the best description of the system. The slightly positive charges on X3 arise from the resonance with structure **B** (vide infra). Structure **A** in Figure 7 represents an ionic structure that does not seem to play an appreciable role.

In line with the idea of closed-shell–closed-shell interactions, and considering the L-shaped molecule as a donor–acceptor molecule, we looked into the intramolecular donor–acceptor interaction between the two closed-shell fragments. We found a strong interaction between the p-type lone pair of X3 of the X_2 unit with the antibonding sigma orbital (σ*) of the AuX unit for all species. This can also be envisioned as resonance between structures **C** and **B**, and the corresponding sigma bond can be considered as a 4-electron 3-center bond. The energy associated with this resonance was estimated by a second-order perturbation approach; it is largest for the iodide (79 kcal mol^{-1}) and decreases toward the fluoride, for which it is 28 kcal mol^{-1} (see Table 5).[47] Separation of the total interaction between these two fragments (AuX and X_2) shows that mostly the orbitals of the X_2 fragment represent the donor orbitals and the AuX orbitals the acceptor orbitals. The overall charge transfer from the X_2 unit to the AuX unit is largest for AuI_3 and decreases along I > Br > Cl, with a charge transfer in the opposite direction (AuF → F_2) for the fluorine species (see Table 5). Landis and co-workers have developed a valence-bond model that works very well in predicting molecular shapes not only for main group elements but also for molecules of transition metals.[48] Their prediction is in agreement with our findings. Strong ionic–covalent resonance rationalizes "hypervalent" bonding; such resonances are usually largest for a linear arrangement of the electron-pair bond and the electron pair localized on the ligand.

Table 5 also lists the bond orders (BO) in the L-shaped trihalides. The covalent BO for the Au–X3 bond is less than half of the value for the Au–X2 bond, thus indicating that structure **C** should have a larger weight in the resonance scheme. The estimated natural localized molecular orbital

0947-6539/01/0717-3666 $ 17.50+.50/0 *Chem. Eur. J.* **2001**, *7*, No. 17

Table 5. Bond orders, donor–acceptor interactions [kcal mol^{-1}], charge transfer [q_{ct} in e],[a] and orbital energies [au][b] in L-shaped AuX_3 molecules.

	F	Cl	Br	I
bond order				
Au1–X2	0.4383	0.4518	0.4893	0.5446
Au1–X3	0.1150	0.2005	0.2147	0.2256
X3–X4	0.8675	0.8705	0.8655	0.8678
donor–acceptor interactions				
$\Sigma E^{(2)}$ [X2–Au1 → X3–X4]	6.41	19.52	26.48	21.88
$\Sigma E^{(2)}$ [X3–X4 → X2–Au1]	39.62	116.63	130.42	127.32
Total $E^{(2)}$	46.03	136.15	156.9	149.20
$E^{(2)}$[p_x-LP(X3) → σ*(Au1–X2)]	27.87	65.63	74.88	78.99
charge transfer				
q_{ct} (XX → AuX)	– 0.0283	0.0493	0.0775	0.1265
HOMO – LUMO gap				
HOMO (X–X), (π_g)	– 0.66139	– 0.45396	– 0.41119	– 0.36280
LUMO (Au–X), (σ)	– 0.03431	– 0.03815	– 0.03727	– 0.03599
gap (HOMO – LUMO)	0.62708	0.41581	0.37392	0.32681

[a] At the B3LYP level. [b] HF orbital energies at the CCSD(T) geometry.

(NLMO) covalent bond orders[49] for the AuX unit decrease as expected from I > Br > Cl > F, with increasing polarization of the Au–X bond. The X3–X4 bond order is almost the same in all species indicating that mainly non-bonding donor orbitals (lone pairs on X_2) are involved in the interaction between the two units.[50]

In the interaction of X_2 with AuX, the LUMO of AuX is an antibonding σ_g* molecular orbital, while the HOMO of X_2 is an antibonding π_g MO, which describes lone-pair electron density. The HOMO – LUMO gap increases in the order I, Br, Cl with the largest gap of about 0.63 au for the AuF/F_2 system. Of course, consideration of only HOMO – LUMO interactions, while being didactic and helpful in understanding the factors leading to certain structures, is an oversimplification; several other orbitals also take part in the Lewis acid/base interaction. Inspection of the molecular orbitals of the L-shaped structure shows a large number of bonding, non-bonding, and antibonding interactions between the two fragments as indicated by a few MOs of AuI_3 in Figure 8. In contrast to the T- and Y-shaped AuX_3 molecules, in which

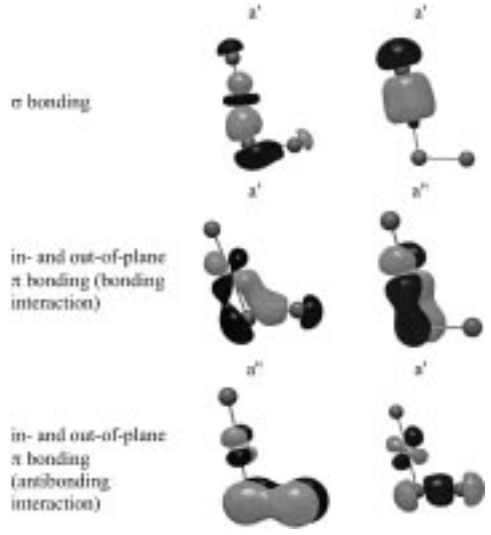

Figure 8. Some of the MOs in L-shaped AuI_3 (HF orbitals at the MP2 geometry).

there was practically no π interaction in the heavier halides (see Figures 4 and 5), there are not only σ-type MOs, but also strong (in- and out-of-plane) π interactions for L-shaped AuI_3 (see Figure 8). The sigma-type MOs mainly involve the 6s and 5d orbitals, while the π-type involve only 5d orbitals on gold.

The donor–acceptor interaction, used above to describe the bonding in L-shaped AuX_3 molecules, is but one example of the so-called closed-shell interactions that have received a great deal of attention in recent years.[4, 51] They comprise all intermolecular interactions, such as hydrogen bonds, donor–acceptor (Lewis acid/base) or charge-transfer bonding, metallophilic interactions, and any other attractive interactions between atoms and molecules. They are especially often encountered with large atoms of which gold and iodine are ideal representatives. Suffice it to mention two examples; one is the $L_3P \cdot I_2$ donor–acceptor complexes, for example, $Ph_3P \times I_2$, in which one of the iodines is attached to P with a charge-transfer bond and has a close to linear P-I-I configuration.[52] In this molecule the I–I bond is considerably longer (3.16(2) Å) than in free iodine, and this can be explained by the fact that electron density shifts from the lone electron pair of phosphorus to a σ* orbital of the iodine molecule. Another example is I_3^-, which was described recently as a donor–acceptor molecule between I_2 and I^-, with I_2 acting as the acceptor and I^- as the donor, just as in $Ph_3P \cdot I_2$.[20] The same authors showed that the bonding in I_3^- could also be described as a hypervalent bond; implying equivalence between the two bond descriptions.

The bonding in the L-shaped AuX_3 molecule is different from the above two examples in that here the X_2 molecule is primarily the donor and the AuX molecule the acceptor. The geometrical parameters show this difference; in the L-shaped AuX_3 system the X–X distance is almost the same as in the free X_2 molecule, for example, r(I–I) = 2.779 in L-AuX_3 versus 2.760 Å in the iodine molecule (CCSD(T)).[50]

The different roles of I_2 in I_3^-, being the acceptor, and in AuI_3, being the donor, are reflected by the differences in the geometries. I_3^- is linear and, as argued by Hoffmann et al.,[20] this indicates that orbital interactions are important in the molecule; the linear shape leads to larger overlap between the p orbital of I^- and the σ orbital of I_2 and, thus, to stronger bonding in the linear configuration. The Au-I-I fragment in our L-shaped AuX_3 molecule is different in this respect. The I_2 molecule acting as the donor and AuI as the acceptor explains the bent shape of the molecule. With bending the molecule, the overlap between the iodine π system and the σ orbital on AuI increases, and this stabilizes the system. The covalent character of the AuX_3 molecule increases from the fluorides towards the iodides, and this is in accord with the fact that the Au-I-I bond angle decreases in this order, from 109° in AuF_3, to 101° in AuI_3.

The bent shape of the Au-I-I fragment can also be explained by the pseudo-Jahn–Teller effect (PJTE). Bersuker et al.[53] have recently studied the I_3 molecule and its positive and negative ions and have shown that the bent shape of I_3 and I_3^+ (in contrast to I_3^-) can be explained by this effect. The PJTE describes the coupling of the ground electronic state (of the linear configuration) with the excited electronic state through bending, which increases the covalent bonding

character of the molecule through new σ – π overlaps. This reasoning applies to the L-shaped AuI_3 molecule as well.

It has been shown recently that metal iodides with excess iodine are capable of replacing polyiodides in crystals.[19] Among others, the $[AuI_2]^- \cdots I_2$ system was found to have an L-shaped structure, essentially similar to that of AuI_3.

Gold monohalide and trihalide dimers

Structure and bonding: We have collected the first consistent set of data for the dimers of gold monohalides and trihalides. The few scattered earlier studies on Au_2F_2,[13, 27] Au_2Cl_2,[14] Au_2X_2 (X = Cl, Br, I),[31] Au_2F_6[13, 15] and Au_2Cl_6[14, 15] are in general agreement with our data. All dimers are planar molecules with two bridging halogen atoms connecting the two monomeric units.

The bridging bonds in all dimers are significantly longer than the corresponding ones in the monomers; this difference decreases gradually from the fluoride toward the iodide, from 0.275 Å in the fluoride to 0.217 Å in the iodide for Au_2X_2. As it was shown previously,[27, 31] relativistic effects reduce the bond lengths of the dimers, but to a lesser extent than in the monomers, by 0.090 and 0.148 Å in Au_2F_2 and Au_2Cl_2, respectively. Comparison of the monomer and dimer bond lengths for the trihalides is more difficult because of the two different types of bond lengths in the monomer trihalides and their changing shape as going from the trifluoride to the triiodide. For these dimers comparison of the terminal and bridging bonds within the same molecule is of interest. This difference (bridging/terminal) decreases from the trifluorides to the triiodides from 0.16 Å in Au_2F_6 to 0.07 Å in Au_2I_6. The latter is unusually small, which may indicate that neither AuI_3 nor Au_2I_6 is very stable.

The most interesting feature of the Au_2X_2 dimers is their extremely short Au ··· Au distance. This is the result of the well-known aurophilic interaction, which is one of the typical examples of the strong closed-shell interactions.[4] The aurophilic interaction is especially pronounced with soft ligands, and generally with larger atoms as observed earlier with numerous complexes.[4] Our results for the Au_2X_2 dimers is in agreement with this observation; the Au ··· Au distance decreases along the series from 2.951 Å in Au_2F_2 to 2.792 Å in Au_2I_2 in accordance with the increasing covalent bond order calculated for Au ··· Au (Table 4). The Au ··· Au distance in Au_2I_2 (2.792 Å) is shorter than the Au–I bond length (2.807 Å). This is in agreement with the earlier results of Schwerdtfeger et al.,[31] who calculated much shorter distances for both, Au ··· Au 2.758 Å versus Au-I 2.787 Å. The gold – gold distance can be expected to be even shorter if larger basis sets on Au are applied, as our trial calculations with two additional f polarization functions indicated (see Table 1). For comparison, the Au – Au bond length in the Au_2 molecule is 2.472 Å from experiment[54] and 2.45,[55] 2.486,[56] and 2.488 Å[57] from computation. The Au ··· Au distance in the zig-zag chain of the gold monoiodide crystal is 3.08 Å, with a Au–I bond length of 2.62 Å.[43]

The Au ··· Au distance decreases with increasing Au–X distances going from F to I, and this results in a substantial opening of the X-Au-X angles along the series, from 97.1° in Au_2F_2 to 120.4° in Au_2I_2. In contrast, the endocyclic bond angles in the Au_2X_6 molecules show constancy at about 87° (except 79° in Au_2F_6) and their Au ··· Au distances increase, accordingly, from the fluorides towards the iodides. These distances are also considerably longer than in the dimers of the monohalides. The more normal behavior is the result of several factors, among them the enhanced role of d orbitals in the valence shell in the trihalides and their decreasing stability towards the heavier halogens. However, in Au_2F_6 and Au_2Cl_6, even the trihalide dimers have a certain amount of direct interaction between the gold atoms in the central ring, as indicated by their molecular orbitals in Figure 9, but much less than in the Au_2X_2 molecules.

The major difference between the Au_2X_2 and Au_2X_6 dimers is that in the former there are both σ- and π-type molecular orbitals participating in the Au ··· Au interaction; while in the latter only σ-type Au ··· Au overlaps are found (see, Figure 9). The two MOs (a_g and b_{3u}) represent four-center bonds for Au_2F_2 and Au_2Cl_2 with rather large coefficients on the halogen. At the same time these MOs look like two-center Au ··· Au interactions in Au_2Br_2 and Au_2I_2, with the halogen coefficients being almost zero. In these last two molecules the maximum of the electron density is in the middle of the Au ··· Au axis, and this is in accord with finding the shortest gold – gold distances in the two heavier Au_2X_2 molecules. Although there are π-type MOs in the Au_2X_6 molecules as well, the overlap is almost zero. There is an almost constant 5d population of 9.92 – 9.93 e in Au_2X_2, while the 5d population in Au_2X_6 increases from 8.91 e in Au_2F_6 to 9.60 e in Au_2I_6. The

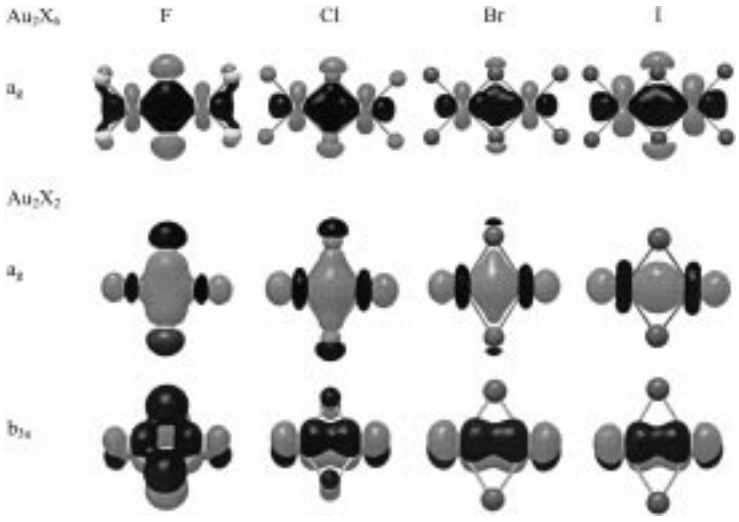

Figure 9. Molecular orbitals showing intra-ring Au ··· Au interactions in Au_2X_2 and Au_2X_6 (HF orbitals at the MP2 geometry).

0947-6539/01/0717-3668 $ 17.50+.50/0 *Chem. Eur. J.* **2001**, *7*, No. 17

6s population increases in both species from the fluorides to the iodides (Table 4). The electronic populations of the T-shaped monomer and the dimer are almost identical, whereas in Au_2X_2 a smaller 6s but a larger 5d population is found than in the monomers. It is interesting to note that the partial charge difference of gold between Au_2X_2 (formal gold(I)) and Au_2X_6 (formal gold(III)) molecules decreases from 0.8 in the fluorides to 0.1 in the iodides.

Dimerization and decomposition: Reaction energies, temperature corrected enthalpies, and Gibbs free energies of several decomposition and dimerization reactions are given in Table 2. Both dimerizations are exothermic, but the energy gain in the dimerization of AuX_3 is much larger, by about 53 (AuF_3) to 10 kcal mol^{-1} (AuI_3), than that of AuX (CCSD(T)). The dimerization energy of AuX_3 decreases for the heavier halogens; the opposite trend was found for the dimerization of AuX, indicating the change in relative stability from AuF_3 (more stable than AuF) to AuI_3 (less stable than AuI) in the solid state. Our computational results are in accord with this. All decomposition reactions of AuX_3 (to $AuX + X_2$) were estimated to be endothermic but decreasingly from AuF_3 to AuI_3 (58 vs 7 kcal mol^{-1}). It should be noted that the computations were carried out for the isolated (gas-phase) species, thus certain differences from solid-state experimental data can be expected. Hence solid-state (lattice and solvents) effects may be responsible for the instability of AuI_3 with respect to its spontaneous decomposition into AuI and I_2.

Acknowledgement

We thank Mr. B. Réffy for drawing the PESs for the trihalides. This work was supported by the Hungarian Scientific Research Fund (Grant No. OTKA T 025788). A.S. thanks Prof. T. M. Klapötke (LMU Munich) for his generous support and Prof. Michael Dolg (University of Bonn) and Dr. I. Frank (LMU Munich) for helpful discussions. We also appreciate the helpful suggestions by one of the referees.

[1] P. Pyykkö, *Chem. Rev.* **1988**, *88*, 563.
[2] P. Pyykkö, J. Li, N. Runeberg, *Chem. Phys. Lett.* **1994**, *218*, 133.
[3] a) F. Scherbaum, A. Grohmann, B. Huber, C. Krueger, H. Schmidbaur, *Angew. Chem.* **1988**, *100*, 1602; *Angew. Chem. Int. Ed. Engl.* **1988**, *27*, 1544; b) H. Schmidbaur, *Gold Bull.* **1990**, *23*, 11.; c) P. Pyykko, N. Runeberg, F. Mendizabal, *Chem. Eur. J.* **1997**, *3*, 1451; d) S.-G. Wang, W. H. E. Schwarz, *Angew. Chem.* **2000**, *112*, 1827; *Angew. Chem. Int. Ed.* **2000**, *39*, 1757.
[4] P. Pyykkö, *Chem. Rev.* **1997**, *97*, 597.
[5] H. A. Jahn, E. Teller, *Proc. R. Soc. London Sect. A* **1937**, *161*, 220.
[6] I. B. Bersuker, V. Z. Polinger, *Vibronic Interactions in Molecules and Crystals*, Springer, Berlin, **1989**.
[7] I. B. Bersuker, *Electronic Structure and Properties of Transition Metal Compounds*, Wiley, New York, **1996**.
[8] V. G. Solomonik, J. E. Boggs, J. F. Stanton, *J. Phys. Chem. A* **1999**, *103*, 838.
[9] H. Koizumi, I. B. Bersuker, *Phys. Rev. Lett.* **1999**, *83*, 3009.
[10] H. Koizumi, I. B. Bersuker, J. E. Boggs, V. Z. Polinger, *J. Chem. Phys.* **2000**, *112*, 8470.
[11] M. C. P. Moate, C. M. O'Brien, J. L. Dunn, C. A. Bates, Y. M. Liu, V. Z. Polinger, *Phys. Rev. Lett.* **1996**, *77*, 4362.
[12] M. Hargittai, B. Réffy, M. Kolonits, C. J. Marsden, J.-L. Heully, *J. Am. Chem. Soc.* **1997**, *119*, 9042.
[13] B. Réffy, M. Kolonits, A. Schulz, T. M. Klapötke, M. Hargittai, *J. Am. Chem. Soc.* **2000**, *122*, 3127.
[14] M. Hargittai, A. Schulz, B. Réffy, M. Kolonits, *J. Am. Chem. Soc.* **2001**, *123*, 1449.
[15] a) P. Schwerdtfeger, P. D. W. Boyd, S. Brienne, A. K. Burrell, *Inorg. Chem.* **1992**, *31*, 3411; b) P. Schwerdtfeger, H. Schmidbaur, *Z. Anorg. Allg. Chem.* **2000**, *626*, 374.
[16] a) G. Herzberg, H. C. Longuet-Higgins, *Discuss. Faraday Soc.* **1963**, *35*, 77; b) T. Carrington, *Acc. Chem. Res.* **1974**, *7*, 20; c) H. Köppel, W. Domcke, L. S. Cederbaum, *Adv. Chem. Phys.* **1984**, *57*, 59–246; d) M. Baer, R. Englman, *Mol. Phys.* **1992**, *75*, 293.
[17] In Ref. [13] the symmetry of the D_{3h}-symmetry structures is given incorrectly, in that it refers to the lower symmetry PES at the intersection. A later note (B. Reffy, M. Kolonits, A. Schulz, T. M. Klapoetke, M. Hargittai, *J. Am. Chem. Soc.* **2001**, *123*, 1545) corrected this error. Unfortunately, the last sentence of the original paper, saying that the D_{3h} symmetry structure has two imaginary frequencies, was overlooked at this stage—while it was correct in the lower symmetry description, it is, of course, no longer valid for the D_{3h} symmetry PES.
[18] T. A. Barckholtz, T. A. Miller, *J. Phys. Chem. A* **1999**, *103*, 2321.
[19] P. H. Svensson, J. Rosdahl, L. Kloo, *Chem. Eur. J.* **1999**, *5*, 305.
[20] G. A. Landrum, N. Goldberg, R. Hoffmann, *J. Chem. Soc. Dalton Trans.* **1997**, 3605.
[21] P. Schwerdtfeger, J. S. McFeaters, R. L. Stephens, M. J. Liddell, M. Dolg, B. A. Hess, *Chem. Phys. Lett.* **1994**, *218*, 362.
[22] D. Schröder, J. Hrusák, I. C. Tornieporth-Oetting, T. M. Klapötke, H. Schwarz, *Angew. Chem.* **1994**, *106*, 223; *Angew. Chem. Int. Ed. Engl.* **1994**, *33*, 212.
[23] C. J. Evans, M. C. L. Gerry, *J. Am. Chem. Soc.* **2000**, *122*, 1560.
[24] M. Hargittai, M. Kolonits, unpublished results.
[25] C. J. Evans, M. C. L. Gerry, *J. Mol. Spectrosc.* **2000**, *203*, 105.
[26] L. C. O'Brien, A. L. Elliott, M. Dulick, *J. Mol. Spectrosc.* **1999**, *194*, 124.
[27] P. Schwerdtfeger, J. S. McFeaters, M. J. Liddell, J. Hrusak, H. Schwarz, *J. Chem. Phys.* **1995**, *103*, 245.
[28] M. Ilias, P. Furdik, M. Urban, *J. Phys. Chem. A* **1998**, *102*, 5263.
[29] P. Schwerdtfeger, M. Dolg, W. H. E. Schwarz, G. A. Bowmaker, P. D. W. Boyd, *J. Chem. Phys.* **1989**, *91*, 1762.
[30] P. Schwerdtfeger, *Mol. Phys.* **1995**, *86*, 359.
[31] P. Schwerdtfeger, A. E. Bruce, M. R. M. Bruce, *J. Am. Chem. Soc.* **1998**, *120*, 6587.
[32] P. Pyykkö, F. Mendizabal, *Inorg. Chem.* **1998**, *37*, 3018.
[33] N. N. Greenwood, A. Earnshaw, *Chemistry of the Elements*, Pergamon Press, Oxford, 1984. p. 1375.
[34] J. H. Choy, Y. I. Kim, S. J. Hwang, P. V. Huong, *J. Phys. Chem. B* **2000**, *104*, 7273.
[35] E. S. Clark, D. H. Templeton, C. H. MacGillavry, *Acta Crystallogr.* **1958**, *11*, 284.
[36] K.-P. Lörcher, J. Strähle, *Z. Naturforsch. Teil. B* **1975**, *30*, 662.
[37] M. Hargittai, *Chem. Rev.* **2000**, *100*, 2233.
[38] a) F. W. B. Einstein, P. R. Rao, J. Trotter, N. Bartlett, *J. Chem. Soc. A* **1967**, 478; b) B. Zemva, K. Lutar, A. Jesih, W. J. Casteel, A. P. Wilkinson, D. E. Cox, R. B. Von Dreele, H. Borrmann, N. Bartlett, *J. Am. Chem. Soc.* **1991**, *113*, 4192.
[39] M. J. Frisch, G. W. Trucks, H. B. Schlegel, G. E. Scuseria, M. A. Robb, J. R. Cheeseman, V. G. Zakrzewski, J. A. Montgomery, Jr., R. E. Stratmann, J. C. Burant, S. Dapprich, J. M. Millam, A. D. Daniels, K. N. Kudin, M. C. Strain, O. Farkas, J. Tomasi, V. Barone, M. Cossi, R. Cammi, B. Mennucci, C. Pomelli, C. Adamo, S. Clifford, J. Ochterski, G. A. Petersson, P. Y. Ayala, Q. Cui, K. Morokuma, D. K. Malick, A. D. Rabuck, K. Raghavachari, J. B. Foresman, J. Cioslowski, J. V. Ortiz, B. B. Stefanov, G. Liu, A. Liashenko, P. Piskorz, I. Komaromi, R. Gomperts, R. L. Martin, D. J. Fox, T. Keith, M. A. Al-Laham, C. Y. Peng, A. Nanayakkara, C. Gonzalez, M. Challacombe, P. M. W. Gill, B. Johnson, W. Chen, M. W. Wong, J. L. Andres, C. Gonzalez, M. Head-Gordon, E. S. Replogle, J. Pople, *Gaussian 98*, *Revision A.6*, Gaussian, Pittsburgh PA, 1998.
[40] a) D. Andrae, U. Häussermann, M. Dolg, H. Stoll, H. Preuss, *Theor. Chim. Acta* **1990**, *77*, 123; b) "Effective Core Potentials": M. Dolg, in *Modern Methods and Algorithms of Quantum Chemistry*, *Vol. 3*, Proceedings, 2nd ed. (Ed.: J. Grotendorst), John von Neumann, Institute for Computing, Jülich, NIC Series, **2000**, pp. 507–540, 2000.

[41] a) C. W. Bauschlicher, H. Partridge, *Chem. Phys. Lett*. **1994**, *231*, 277; b) A. D. Becke, *J. Chem. Phys*. **1993**, *98*, 5648; c) A. D. Becke, *Phys. Rev. A* **1988**, *38*, 3098; d) C. Lee, W. Yang, R. G. Parr, *Phys. Rev. B*, **1988**, *37*, 785; e) S. H. Vosko, L. Wilk, M. Nusair, *Can. J. Phys*. **1980**, *58*, 1200.

[42] a) "NBO Version 3.1": E. D. Glendening, A. E. Reed, J. E. Carpenter, F. Weinhold, *J. Mol. Struct. (THEOCHEM)* **1988**, *169*, 41; c) J. P. Foster, F. Weinhold, *J. Am. Chem. Soc.* **1980**, *102*, 7211; d) A. E. Reed, F. Weinhold, *J. Chem. Phys.* **1983**, *78*, 4066; e) A. E. Reed, R. B. Weinstock, F. Weinhold, *J. Chem. Phys.* **1985**, *83*, 735; f) A. E. Reed, L. A. Curtiss, F. Weinhold, *Chem. Rev.* **1988**, *88*, 899; g) A. E. Reed, P. von R. Schleyer, *J. Am. Chem. Soc.* **1987**, *109*, 7362; h) A. E. Reed, P. von R. Schleyer, *Inorg. Chem.* **1988**, *27*, 3969; i) F. Weinhold, J. E. Carpenter, *The Structure of Small Molecules and Ions*, Plenum, **1988**, p. 227.

[43] H. Jagodzinski, *Z. Kristallogr*. **1959**, *112*, 80.

[44] Pseudo-Jahn–Teller effect occurs when two electronic states mix through vibronic coupling. Thus even a nondegenerate ground state may become unstable if the vibronic coupling to a close-lying excited state is strong. For more detail see, for example, refs. [6] and [7]. The pseudo-Jahn–Teller effect is often referred to, incorrectly, as "second-order Jahn–Teller effect."

[45] H. Köppel, W. Domcke, L. S. Cederbaum, *Adv. Chem. Phys.* **1984**, *57*, 150.

[46] A. Schulz, *Trends Inorg. Chem.* **1999**, *6*, 137.

[47] NBO analysis: The second-order perturbation energy was computed according to $\Delta_{\varphi\varphi^*}E^{(2)} = -2(\langle\varphi\,|\,h^F\varphi^*\rangle)^2/(\varepsilon_{\varphi^*} - \varepsilon_{\varphi})$ with h^F being the Fock operator.

[48] a) C. R. Landis, T. K. Firman, D. M. Root, T. Cleveland, *J. Am. Chem. Soc.* **1998**, *120*, 1842; b) C. R. Landis, T. Vleveland, T. K. Firman, *J. Am. Chem. Soc.* **1998**, *120*, 2641.

[49] Natural localized molecular orbital (NLMO) bond orders of the NBO analysis; A. E. Reed, P. von R. Schleyer, *J. Am. Chem. Soc*. **1990**, *112*, 1434 and also Ref. [42h].

[50] The energy associated with the "opposite" type of interaction, that is, the AuX donor orbitals with the empty σ* X3−X4 acceptor orbital is less than 5 kcal mol^{-1} for all species, in agreement with the X3−X4 bond orders. This is so small that this type of donor–acceptor interaction has only a minor effect on the X3−X4 bond length.

[51] G. Desiraju, *J. Chem. Soc. Dalton Trans.* **2000**, 3745.

[52] S. M. Gondfrey, D. G. Kelly, C. A. McAuliffe, A. G. Mackie, R. G. Pritchard, S. M. Watson, *J. Chem. Soc. Chem. Commun*. **1991**, 1163.

[53] N. N. Gorinchoi, F. Cimpoesu, I. B. Bersuker, *J. Mol. Struct. (THEOCHEM)* **2000**, *530*, 281.

[54] K. P. Huber, G. Herzberg, *Molecular Spectra and Molecular Structure*, *IV: Constants for Diatomic Molecules*, Van Nostrand, New York, **1979**.

[55] M. Barysz, P. Pyykkö, *Chem. Phys. Lett*. **2000**, *325*, 225.

[56] R. Wesendrup, J. K. Laerdahl, P. Schwerdtfeger, *J. Chem. Phys.* **1999**, *110*, 9457.

[57] B. A. Hess, U. Kaldor, *J. Chem. Phys.* **2000**, *112*, 1809.

Received: February 20, 2001 [F3086]

  0947-6539/01/0717-3670 $ 17.50+.50/0